Numerical simulation of charge transport in disordered organic semiconductor devices

E. Knapp,[1,a)] R. Häusermann,[1] H. U. Schwarzenbach,[1] and B. Ruhstaller[1,2,b)]
[1]*Institute of Computational Physics, Zurich University of Applied Sciences, Wildbachstrasse 21, 8401 Winterthur, Switzerland*
[2]*Fluxim AG, Dorfstrasse 7, 8835 Feusisberg, Switzerland*

(Received 26 December 2009; accepted 9 July 2010; published online 7 September 2010)

For the design of organic semiconductor devices such as organic light-emitting devices and solar cells, it is of crucial importance to solve the underlying charge transport equations efficiently and accurately. Only a fast and robust solver allows the use of fitting algorithms for parameter extraction and variation. Introducing appropriate models for organic semiconductors that account for the disordered nature of hopping transport leads to increasingly nonlinear and more strongly coupled equations. The solution procedures we present in this study offer a versatile, robust, and efficient means of simulating organic semiconductor devices. They allow for the direct solution of the steady-state drift-diffusion problem. We demonstrate that the numerical methods perform well in combination with advanced physical transport models such as energetic Gaussian disorder, density-dependent and field-dependent mobilities, the generalized Einstein diffusion, traps, and its consistent charge injection model. © *2010 American Institute of Physics*. [doi:10.1063/1.3475505]

I. INTRODUCTION

Soon after the invention of organic light-emitting devices (OLEDs),[1,2] theoretical models for describing charge transport and recombination have been derived.[3–5] Detailed models of device behavior are required to optimize the efficiency and performance of organic devices. For solving these models, several numerical methods have been introduced and used so far, of which three are known best. The first method is based on a Monte Carlo algorithm. The Monte Carlo simulation considers site energies that are random variables leading to hopping processes on a microscopic level. This simulation method offers a direct theoretical approach but is very time consuming. Therefore, it is usually applied to carrier transport studies in the bulk of organic materials[6] and only recently to more complex multilayer devices. The second method which is based on "hopping transport" solves a probability evolution equation, known as the master equation.[7,8] The third method is based on the continuum approach and presented in this paper. It is called the drift-diffusion model. As with inorganic devices, a series of highly nonlinear coupled partial differential equations (PDEs) describes the injection, transport, and recombination dynamics of charge carriers in organic devices. Without any simplifying assumptions these equations cannot be solved analytically. The commercially available software packages for simulating charge transport have usually been developed for inorganic semiconductor materials. However, organic semiconductors differ considerably from their inorganic counterparts, not only by low carrier mobilities, static dielectric constants, and long recombination times but also by the disorder. Taking the disordered nature of organic materials into account leads to a description in terms of a Gaussian density of states (DOS) which affects the mobility of charge carriers and the diffusion coefficient. The Gaussian DOS and the extended Gaussian disorder model (EGDM) (Ref. 9) with field and density dependence enhance the nonlinearities and the coupling between the equations. These circumstances hinder the use of standard drift-diffusion solvers.

Due to the simple device geometry in OLEDs, a one-dimensional (1D) transport model consisting of drift and diffusion has usually been solved. Generally, the drift-diffusion problem is solved time-dependently in a decoupled manner.[10–13] Pflumm[14] and deMello[15] adapted or replaced Poisson's equation with a time-dependent version and solved the system in a coupled and time-dependent manner. Additionally, deMello applied an adaptive mesh as opposed to the widely known Scharfetter–Gummel discretization at the cost of having additional criteria to be evaluated. Moreover, decoupled steady-state solvers were applied to simulate organic solar cells and OLEDs.[16,17] Further, van Mensfoort and Coehoorn[9] developed a continuum approach based on the Bohnham and Jarvis method[18,19] which, however, is limited to unipolar devices.

Since for parameter extraction from current-voltage curves only the steady-state solution is of interest and the evolution of the physical quantities in time is not required, we solve the drift-diffusion problem for organic semiconductors in a coupled manner directly for the steady-state. This yields the advantage of faster convergence than the decoupled or time-dependent methods. Moreover, the method can deal with bipolar as well as multilayer devices.

We will restrict ourselves to the basic set of drift-diffusion equations consisting of the electron and hole continuity and Poisson's equation. It is clear that a full OLED or organic photovoltaics model will also have to deal with the rate equation for excitons and energy transfer among them.

[a)]Electronic mail: evelyne.knapp@zhaw.ch.
[b)]Electronic mail: beat.ruhstaller@zhaw.ch.

This, however, leads to an extension of the model that will not affect the choice of the numerical methods presented here.

II. TRANSPORT MODEL

In this section, we introduce the drift-diffusion equations. The physical models for organic semiconductors for charge transport are presented as well as consistent boundary conditions.

A. Basic drift-diffusion model

For the description of charge transport in OLEDs the general semiconductor drift-diffusion equations for electrons and holes are valid. In Poisson's equation

$$\nabla \cdot (\epsilon \nabla \psi) = q(n_f + n_t - p_f - p_t), \tag{1}$$

the electrical potential ψ is related to the electron and hole densities n and p, where q is the elementary charge and ϵ is the product of the vacuum permittivity ϵ_0 and the relative permittivity ϵ_r of the organic material. The carrier densities $n=n_f+n_t$ and $p=p_f+p_t$ consist of mobile charge carriers n_f and p_f as well as trapped charges n_t and p_t.

The current equations for electrons and holes are determined by the mobile carriers and read

$$J_n = -qn_f\mu_n \nabla \psi + qD_n \nabla n_f,$$

$$J_p = -qp_f\mu_p \nabla \psi - qD_p \nabla p_f. \tag{2}$$

The current density consists of a drift part caused by the electric field and a diffusion current. The mobility $\mu_{n,p}$ is dependent on the field, temperature and density. It thus depends on the position. The total current in the device is the sum of the electron and hole current $J=J_n+J_p$. The diffusion coefficient $D_{n,p}$ is given by the generalized Einstein relation as discussed further below. The conservation of charges leads to the continuity equations for electrons and holes

$$\nabla \cdot J_n - q\left(\frac{\partial n}{\partial t}\right) = qR(n_f,p_f),$$

$$\nabla \cdot J_p + q\left(\frac{\partial p}{\partial t}\right) = -qR(n_f,p_f), \tag{3}$$

where R denotes the bimolecular recombination rate given by Langevin[20] and t the time. These equations take charge migration and recombination into account. The time derivative in Eq. (3) is omitted in the following due to the steady-state analysis of this paper.

B. Physical models of disordered organic semiconductors

In organic materials the disorder caused by the molecular structure is described by a Gaussian DOS

$$N_{Gauss}(E) = \frac{N_0}{\sqrt{2\pi\sigma^2}} \exp\left[-\left(\frac{E-E_0}{\sqrt{2}\sigma}\right)^2\right], \tag{4}$$

where σ denotes the disorder parameter ranging from 50 to 150 meV. The parameter N_0 stands for the site density and the parameter E_0 denotes the reference energy level.

Traps are taken into account by a superposition of the Gaussian DOS for free charge carriers and an exponential DOS

$$N_{Exp}(E) = \frac{N_{Trap}}{kT_0} \exp\left[\frac{E}{kT_0}\right], \tag{5}$$

with $E \leq 0$ for trapped carriers. Equation (5) contains two parameters, namely the characteristic temperature T_0 and the density of available trap states N_{Trap}. Note that the exponential distribution has no offset to the center of the Gaussian DOS.

The carrier density for free and trapped charges is determined by

$$p(E_f) = \int_{-\infty}^{\infty} N(E) f(E,E_f) dE \tag{6}$$

where f stands for the Fermi–Dirac distribution, $N(E)$ for the DOS, and E_f for the Fermi energy.

The disorder in organic semiconductors also affects the mobility law. The EGDM (Ref. 9) is an extension of the Pasveer model[21] by additionally considering diffusion effects. In the EGDM the mobility may be expressed according to van Mensfoort and Coehoorn[9] as a product of a density-dependent and field-dependent factor

$$\mu(T,p_f,F) = \mu_0(T) g_1(p_f,T) g_2(F,T), \tag{7}$$

with the enhancement functions $g_1(p_f,T)$ and $g_2(F,T)$. They account for the influence of the charge density, the electric field and the energetic disorder. The functions $g_1(p_f,T)$ and $g_2(F,T)$ are nonlinear and strongly increase with larger values of the disorder parameter.[9]

In the EGDM the Gaussian DOS also influences charge diffusion. Roichman, Preezant, and Tessler[22,23] pointed out that the use of the generalized instead of the classical Einstein relation is correct. In this case the generalized Einstein diffusion coefficient is thus determined by[9]

$$D = \frac{kT}{q} \mu(T,p_f,F) g_3(p_f,T), \tag{8}$$

where the enhancement function $g_3(p_f,T)$ reads

$$g_3(p_f,T) = \frac{1}{kT} \frac{p_f}{\frac{\partial p_f}{\partial E_f}}. \tag{9}$$

C. Boundary conditions

We use Dirichlet boundary conditions for the charge densities and the potential at the anode and cathode. An effective potential of $V_{eff}=V_{app}-V_{bi}$ is imposed at the electrodes where V_{app} denotes the applied voltage and V_{bi} the built-in potential which in turn is determined as the difference of the electrode work functions. The charge injection into the organic semiconductor is dependent on the energetic barrier that carriers have to overcome to enter the bulk. According to the original description by Emtage and O'Dwyer,[24] this barrier is lowered due to the image potential

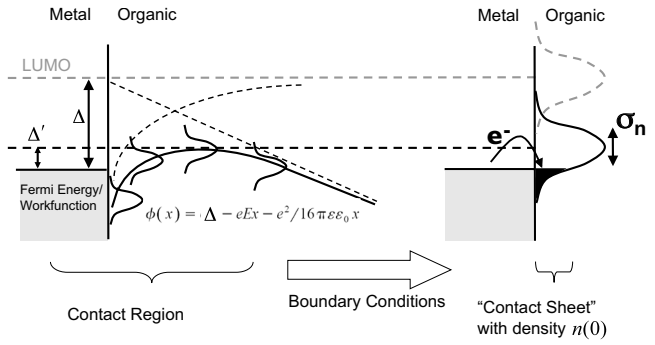

FIG. 1. Illustration of the injection barrier reduction and filling of the Gaussian DOS. The image potential and the applied electric field lower the nominal barrier and define the position of the center of the Gaussian DOS.

that is generated when a carrier enters the bulk and the applied external field as shown in Fig. 1. The lowered barrier in the contact region can be described as a boundary condition in the contact sheet. The center of the Gaussian DOS is thus aligned with the reduced barrier. This model can be considered as an extension of the ones presented in Refs. 3 and 24 for the situation of a disordered semiconductor with a Gaussian DOS. Alternatively as motivated by the right sketch of Fig. 1 this injection can be interpreted as charge carrier diffusion from the metal into the tail of the DOS. Thus the values for the carrier densities at the anode and cathode satisfy Eq. (6). The densities at the boundaries are updated in each iteration of the algorithm until self-consistency is reached.

III. NUMERICAL SOLUTION METHODS

Solving the system of partial differential Eqs. (1)–(3) with the model ingredients Eqs. (7) and (8) in consideration of the boundary conditions leads to a system of highly nonlinear equations. The enhancement functions of the EGDM and the generalized Einstein relation $g_1(p_f,T)$, $g_2(F,T)$, and $g_3(p_f,T)$ pronounce the nonlinearities and the mobility model increases the coupling between the equations. Especially large values of the disorder parameter σ or a low temperature T increase these effects. Therefore, we have developed, implemented, and tested suitable numerical methods.

A. Discretization method

To tackle the drift-diffusion Eqs. (1) and (3) numerically, the device is divided into $n+1$ grid points and the corresponding finite volumes as shown in Fig. 2. We use a uniform grid with the points $x_0,\ldots,x_n$, the mesh elements $[x_i,x_{i+1}]$ and the finite volumes $[x_{i-1/2},x_{i+1/2}]$. The 1D simulation domain is restricted to the organic material.

The discretized equations are solved in every grid point

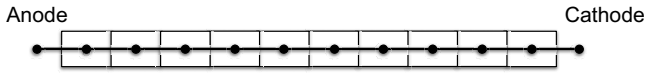

FIG. 2. Illustration of the spatial discretization. The grid consists of $n+1$ grid points which results in $n-1$ boxes.

in the domain for the three degrees of freedom, namely, the potential ψ, the electron and hole densities n_f and p_f. On the grid points the densities and the potential are calculated while on the edge of the boxes the values for the electric current and field are determined. By reformulating Eqs. (1) and (3) and arranging all terms to the same side, a system of equations denoted by

$$F(u) = 0, \tag{10}$$

is obtained with $u=(\psi,p_f,n_f)$. The vector of residuals $F=(F_1,F_2,F_3)$ consists of F_1 that denotes the discretization of Poisson's equation, F_2 the continuity equations for holes and F_3 the continuity equations for electrons. The goal of the numerical approximation is to satisfy Eq. (10) as accurately as possible.

For the finite volume discretization the steady-state versions of Eqs. (1)–(3) are integrated over a finite volume $[x_{i-1/2},x_{i+1/2}]$, then Gauss' theorem is applied which results in the discretization of Poisson's and the continuity equations. With this discretization method the current conservation within the device is guaranteed. However, special attention is paid to the discretization of the current Eq. (2) for which the Scharfetter–Gummel discretization[25] has been introduced in semiconductor modeling. It helps to accurately describe steep changes in carrier densities, even on a coarse grid. In case of a large, normalized disorder parameter $\hat{\sigma}=\sigma/(kT)$, the mobility and the diffusion coefficient can vary strongly within an element and hence a grid refinement might be appropriate.

B. Initial guess

Usually, an empty device[26] with no charge carrier is used as a starting point for a simulation. This, however, does not correspond to the physical situation and an additional simulation run prior to the simulation of interest is required to get a reasonable starting point for no externally applied field. Furthermore the convergence of a numerical algorithm is sensitive to the starting point. Thus, a technique for a good starting point is developed in the following.

As a very first starting point for the iterative algorithm introduced below, we make use of the equilibrium condition where no external field is applied. Any material or device in thermodynamic equilibrium will have a constant Fermi level everywhere in the device. Thus the currents J_n and J_p in Eq. (2) are zero. In case of no disorder the Boltzmann statistics is used and $g_3(n_f,T)=1$ in Eq. (9) everywhere in the device. Introducing these properties leads to an equation for electrons (similar for holes) of the form

$$\frac{\partial\psi(x)}{\partial x} = \frac{U_t}{n_f(x)}\frac{\partial n_f(x)}{\partial x}, \tag{11}$$

where U_t is the thermal voltage kT/q. This equation describes the relationship between the electric potential ψ and the electron concentration n_f in case of equilibrium. Hence, Eq. (11) can be solved for the electron density n_f

$$n_f(x) = n_r \exp\left(\frac{\psi(x)}{U_t}\right), \tag{12}$$

where n_r is the electron concentration at the right boundary. The electric potential is defined to be zero there. Due to the equilibrium condition, the continuity Eq. (3) reduce to meaningless identities, assuming there is no recombination. Poisson's Eq. (1) remains valid in its usual form in the equilibrium condition. Substitution of Eq. (12) in Eq. (1) leads to the following equation describing the equilibrium condition in case of a trap-free material:

$$\frac{d^2\psi(x)}{dx^2} + \frac{q}{\epsilon}\left[p_r \exp\left(\frac{-\psi(x)}{U_t}\right) - n_r \exp\left(\frac{\psi(x)}{U_t}\right)\right] = 0. \tag{13}$$

The equilibrium conditions for the potential are imposed as boundary conditions and Eq. (13) can now be solved for the potential. It is notable that the equilibrium state does not depend on the mobility. We extend this procedure for the case of a disordered semiconductor, i.e., $g_3(n_f, T) \geq 1$. Here however, the relationship between the charge carrier density n_f and ψ is of a more complex nature

$$n_f(x) = N_0 \int_{-\infty}^{\infty} \frac{1}{\sqrt{2\pi\sigma}} \exp\left[-\left(\frac{E + E_{offset}}{\sqrt{2}\sigma}\right)^2\right] \frac{1}{1 + \exp\left[-\frac{q}{kT}\{E + [\psi(x) - \phi_e(x)]\}\right]} dE, \tag{14}$$

where N_0 denotes the site density of the Gaussian DOS. The energy E_{offset} describes the offset with respect to the Fermi level lying between the highest occupied molecular orbital (HOMO) and lowest unoccupied molecular orbital. Again, the Fermi level is constant throughout the device in equilibrium. In thermal equilibrium the electron quasi Fermi level ϕ_e and the hole quasi Fermi level ϕ_h and the Fermi level are equal. Poisson's equation with the expressions of the form of Eq. (14) for the electron and hole density is then solved numerically for the potential by means of Newton's algorithm. The effect of traps can also be taken into consideration by accounting for the trapped charges in Poisson's equation. In case of multilayer devices the same procedure is applicable. The physically meaningful initial condition derived this way is self-consistent and helps the convergence of the iterative steady-state algorithms used in this study. Moreover, the same procedure for determining the equilibrium solution can be applied to transient simulations.

C. Newton's method

The discretized Eq. (10) can be solved numerically in a coupled or decoupled manner. The coupled Newton approach linearizes the system of equations and solves it simultaneously. The resulting linear system of equations requires the determination of the Jacobian matrix which can be quite tedious. In case of the physical models as presented in Sec. II B this leads to a more complex form of the Jacobian matrix. During an iteration, the coupling between adjacent grid points and between the three equations is preserved. A good initial guess is crucial for convergence. Close to the solution, Newton's algorithm shows quadratic convergence. In the following an outline of Newton's algorithm is given: We solve the system of three equations in Eq. (10). Using a Taylor series expansion of first order around the point u'

$$F(u') \approx F(u) + F'(u)(u' - u), \tag{15}$$

where $F'(u)$ denotes the Jacobian matrix, the problem can be reformulated as

$$u' \approx u - [F'(u)^{-1}]F(u), \tag{16}$$

with $F(u')=0$. This leads to the iterative scheme

$$u^{k+1} = u^k - [F'(u^k)^{-1}]F(u^k). \tag{17}$$

In practice Eq. (17) is expressed as

$$u^{k+1} = u^k + du^k, \tag{18}$$

where du^k is the solution of the linear system

$$F'(u^k)du^k = -F(u^k). \tag{19}$$

The very first starting point of a current-voltage curve for no applied field is obtained as described in Sec. III B. To have an appropriate starting point is crucial for the algorithm to converge. For the next voltage point of a current-voltage curve, convergence is obtained by starting with the solution of the previous voltage and by increasing the applied voltage. In some cases, damping the update du^k or gradually increasing the disorder parameter $\hat{\sigma}$ may enhance convergence. If the initial value is too far from the true solution, the algorithm may fail to converge. Especially in the case of strong disorder a good initial guess is valuable. Further, the form of the Jacobian matrix in case of the EGDM is quite complicated and thus less straight forward than for the case of a constant mobility and diffusion.

D. Gummel's method

As an alternative to Newton's algorithm, Gummel's approach[27] solves the equations sequentially and, therefore, decoupled. First, Poisson's equation is solved in all grid points, followed by the electron continuity equation and the hole continuity equation. This procedure is repeated until convergence is obtained. In an iteration, the coupling be-

tween neighboring grid points is preserved while the equations are loosely coupled through successive updates of the variables ψ, p_f, and n_f which thus in general converges slower than the fully coupled Newton algorithm.

In this study, we used a steady-state version of Gummel's algorithm. Since Poisson's equation is part of the coupled system of PDEs, the dependence of the charge density on the potential is implicitly accounted for. In the decoupled case the effect of the potential on the carrier density is not included *a priori* in Poisson's equation. Especially in regimes with high carrier density, e.g., at contacts this may lead to oscillations and to divergence of the entire system. According to Gummel[27] the stability of the stationary solver can be improved by taking the approximative variation in the carrier concentration with the potential into account. The stabilized version of Poisson's equation is of the following form[28] where k denotes the number of iterations:

$$\nabla \cdot \frac{\epsilon}{q} \nabla \psi^{k+1} - \left[\frac{n^k + p^k}{U_t} (\psi^{k+1} - \psi^k) \right] - (n^k - p^k) = 0. \quad (20)$$

The additional term in Eq. (20) compared to Eq. (1) enforces the diagonal of the system of equations and prevents thus an overshoot of the solution. The additional term in Poisson's equation can be interpreted as a damping factor. However, only through this modification in Eq. (20) convergence of the decoupled system can be ensured. Note that a converged solution reduces Eq. (20) to Eq. (1). The equations are written in the variable set (ψ, p_f, n_f). The EGDM, as opposed to the case of a constant mobility and diffusion, turns Eq. (2) into a nonlinear equation in the density n_f due to the density-dependent mobility model and generalized Einstein relation. Therefore, the continuity equation in a Gummel iteration must be solved by Newton's algorithm.

IV. VALIDATION OF NUMERICAL ALGORITHMS

To validate the results of the presented algorithms, we compare our results with an example previously studied by van Mensfoort and Coehoorn.[9] Their method, however, is limited to unipolar, single-layer devices. Therefore, a symmetric hole-only device with no injection barrier is simulated. In Fig. 3 current-voltage curves are shown for constant mobility (with diffusion), Mott–Gurney (analytical solution without diffusion), and the full EGDM model in accordance with results from Ref. 9 which are also plotted in the figure. The influence of diffusion is strong at low voltage only. The slope of the EGDM curve increases at high bias due to its field and density dependence.

As a next step in model complexity, we introduce charge injection barriers at the electrodes. Considering energetic disorder in the organic layer next to the charge-injecting electrode, we obtain a device description which consistently accounts for disorder effects. The device length l is set to 22 nm, $\sigma/kT=6$, $N_0=2.44\times10^{26}$ m^{-3}, and $\mu_0=1.1\times10^{-16}$ m^2/V s at room temperature.

Our results for a single-carrier device are shown in Figs. 4 and 5. Both results are in good agreement with calculations by van der Holst[29] who has used a three-dimensional (3D) Master equation approach. In Fig. 4 simulated current-

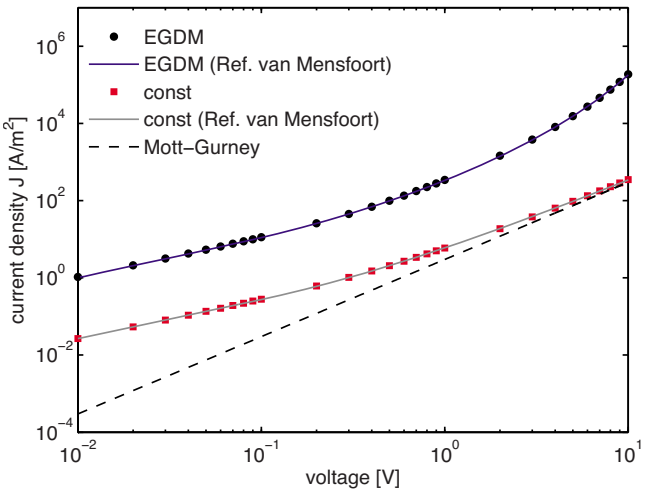

FIG. 3. (Color online) The EGDM solution is shown and compared with the result from van Mensfoort (Ref. 9). The same is done for the constant mobility and diffusion coefficient. As a guide-to-the-eye the Mott–Gurney law is drawn. The effect of diffusion is visible at low voltages. At high voltage the EGDM solution starts to differ from the Mott–Gurney law.

voltage curves for injection barriers ranging from 0, 0.33, and 0.67 to 1 eV are depicted. Figure 5 demonstrates the reduction in the injection current for high barriers and the influence of the image charge for the same device. The driving voltage is set to 2 V. The current density for the EGDM decreases significantly when the injection barrier is higher than 0.5 eV since the partially filled Gaussian DOS limits the injection current (see Fig. 1).

As a next example we show in Fig. 6 simulation results of the EGDM combined with an exponential trap distribution and compare it with the trap-free case. To put the simulation in an experimental context we carry out our simulation for a device from literature. Our simulations are consistent with Ref. 30 where the following parameters and experimental values are taken from: $l=129$ nm, $T=293$ K, injection barrier $\Delta=0.3$ eV, $N_{Trap}=10^{24}$ m^{-3}, $T_0=2100$ K, $N_0=10^{27}$ m^{-3}, $\sigma=0.07$ eV, $\mu_0=10^{-9}$ m^2/(V s), and V_{bi}

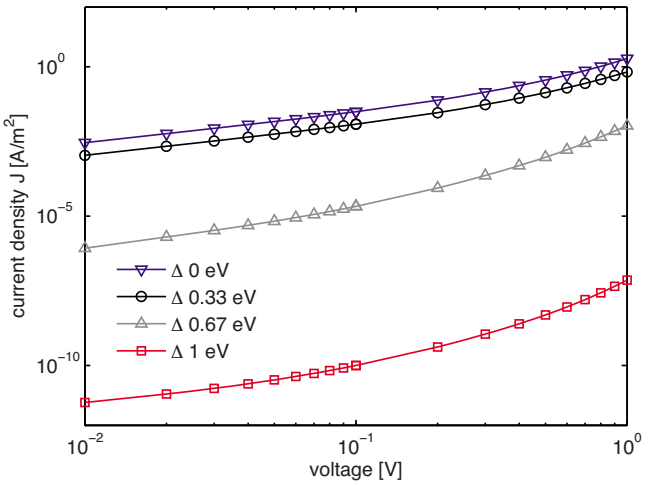

FIG. 4. (Color online) Current-voltage curves have been calculated for different injection barriers. The results agree well with van der Holst (Ref. 29) who obtained the same results by Master equation calculations. Parameters used are: $l=22$ nm, $\sigma/kT=6$, $N_0=2.44\times10^{26}$ m^{-3}, and $\mu_0=1.1\times10^{-16}$ m^2/V s at room temperature.

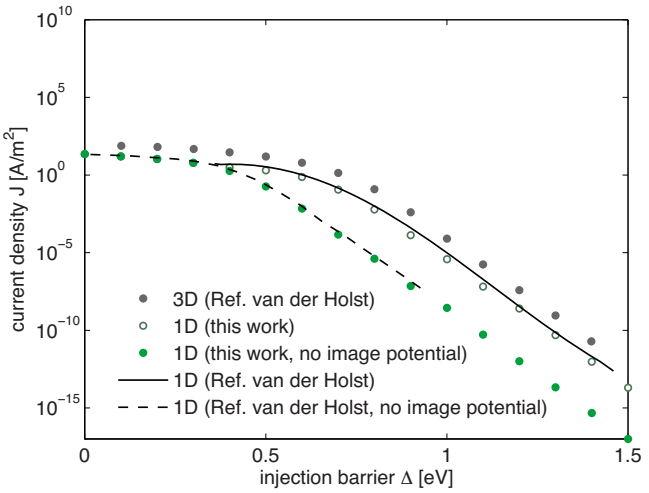

FIG. 5. (Color online) The effect of the injection barrier on the current density is shown in this figure. The results for the 3D master equation and 1D continuum model are taken from van der Holst (Ref. 29) and superposed with our results (open circles and closed circles). The driving voltage in these simulations was set to 2 V. The device configuration is the same as in Fig. 4.

=0.9 V. This demonstrates that the numerical method is able to deal with traps. The simulation is carried out successfully over many orders of magnitude in current and voltage. In case of traps, we observe, as expected, that the current approaches the trap-free case at high bias.

To demonstrate the feasibility of the introduced algorithms and the EGDM for a bipolar OLED, we plot the resulting Langevin recombination profiles in Fig. 7. The following simulation parameters were used: $T=298$ K, $l=100$ nm, $\mu_0=10^{-10}$ m^2/(V s), injection barriers $\Delta_{e,h}=0$ eV, $N_0=10^{27}$ m^{-3}, and $V_{bi}=2$ V.

In this symmetric example holes and electrons have the same mobilities. The recombination profiles have been normalized for visualization such that the integral over the normalized device thickness is equal to one. As a reference the

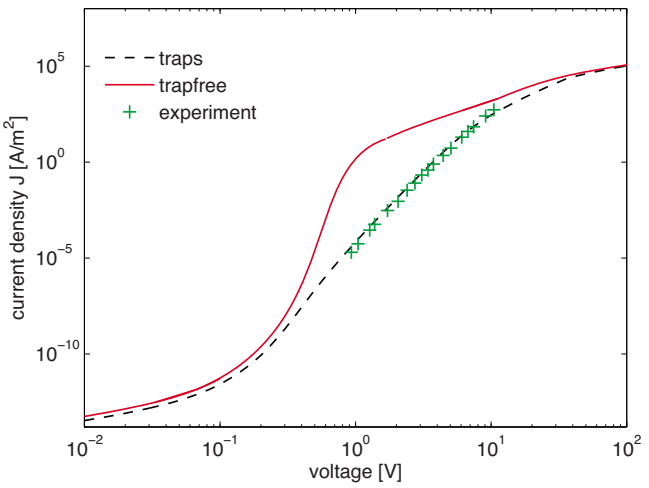

FIG. 6. (Color online) Illustration of trapping effects on a current-voltage curve. The trap-limited current-voltage curve is superposed with a trap-free simulation and experimental data points from Ref. 30. Parameters used are: $l=129$ nm, $T=293$ K, injection barrier $\Delta=0.3$ eV, $N_{Trap}=10^{24}$ m^{-3}, $T_0=2100$ K, $N_0=10^{27}$ m^{-3}, $\sigma=0.07$ eV, $\mu_0=10^{-9}$ m^2/(V s), and $V_{bi}=0.9$ V.

results for constant mobility are plotted. For this case the recombination profiles are rather flat with a maximum in the center of the device. For disorder-enhanced mobilities, the recombination profiles are increased in the center (low voltage case) or near the edges (high-voltage case). Stronger disorder in the organic material enhances the maximal recombination and thus the profiles are more confined. The profiles differ slightly from Ref. 8 where a new Langevin recombination model was applied with an enhanced field dependence.

V. PERFORMANCE OF NUMERICAL ALGORITHMS

Since we directly solve the drift-diffusion problem for the steady-state, the procedure is especially suitable to calculate current-voltage curves in a fast and efficient manner. This is necessary for material characterization based on measured current-voltage data. We benchmark the calculation of a current-voltage curve in terms of number of iterations. We restrict this comparison to Gummel and Newton's method for the steady-state problem. Other methods such as Monte Carlo simulations will require more time since a large number of samples is required for a good statistical result. Also the master equation approach is costly from a computational viewpoint since convergence depends on reaching an equilibrium state by means of hopping rates. The Bonham and Jarvis method presented by Mensfoort is limited to unipolar devices and is thus not versatile enough. We present the benchmarking results of a single-layer hole-only device and its performance. Applying the initial guess strategy from Sec. III B for the constant mobility and disordered case ($\hat{\sigma}=6$) to a hole-only device with length $l=100$ nm, $N_0=10^{27}$ m^{-3}, and a built-in potential of $V_{bi}=1.5$ V and $V_{bi}=2$ V, respectively, we obtain a density profile as shown in Fig. 8. To obtain approximatively the same carrier densities at the cathode we determine different built-in potentials for the constant mobility and the EGDM case. For the constant mobility model, the built-in potential can be determined by $V_{bi}=(kT/q)\times\log(n_1/n_2)$. This formula is derived from $V_{bi}=\phi_2-\phi_1$ and $n_{1,2}=N_0\exp\left[(E_{\mathrm{HOMO}}-\phi_{1,2})\frac{q}{kT}\right]$ where ϕ denotes the work function at the anode and cathode and E_{HOMO} the energy level of the HOMO. For the EGDM the boundary charge density values satisfy Eq. (6).

These profiles serve as starting points for the current-voltage calculations. By stepwise increasing the potential a series of voltage points is computed. We compare the convergence behavior of Gummel and Newton's algorithm for a current-voltage calculation. The number of iterations used for a voltage point is shown in Fig. 9. As a convergence criterion the relative changes in the potential and density from one iteration k to the next have to satisfy

$$\frac{1}{n_V}\left(\left\|\frac{\psi^{k+1}-\psi^k}{\psi^k}\right\|+\left\|\frac{p^{k+1}-p^k}{p^k}\right\|\right)\leq 10^{-10}, \tag{21}$$

where n_V is the length of the vectors ψ and p. For the constant mobility and diffusion coefficient the number of (about five) iterations for Newton's algorithm remains almost the same regardless of the applied voltage. In case of Gummel's algorithm the number of iterations clearly increases with the

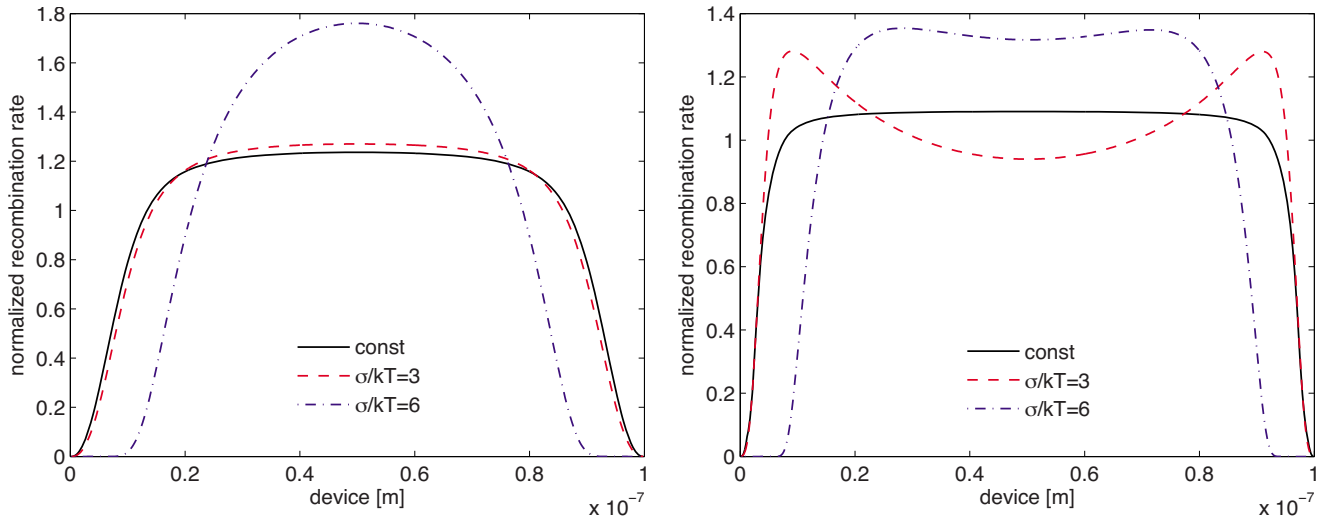

FIG. 7. (Color online) Recombination profiles for constant mobility and different disorder parameters $\hat{\sigma}$ simulated at 3 and 10 V. Parameters were set to $T=298$ K, $l=100$ nm, $V_{bi}=2$ V, $\epsilon_r=3$, $\mu_0=10^{-10}$ m^2/(V s).

applied voltage. This is due to the increased coupling between Poisson's equation and the continuity equation at high bias.

For Newton's algorithm applied to the EGDM the number of iterations does not increase. As opposed to the constant case, especially at low voltage more iterations are required for Gummel's algorithm due to the disorder-affected generalized Einstein relation. Although an iteration is more time consuming in Newton than in Gummel's method a current-voltage calculation is faster with Newton's algorithm as the number of iterations stays low independently of the applied voltage. If we compare the constant mobility and the EGDM case with respect to calculation time the EGDM requires more time since the evaluation of the residuals and the Jacobian matrix is more expensive than in the constant case due to the additional model ingredients and their derivatives. The results of Fig. 9 show that Gummel and especially Newton's algorithm perform well in combination with the novel physical models for current-voltage calculations. For the given current-voltage calculation for the EGDM and constant mobility case we found that Newton's algorithm is at least ten times faster than Gummel's algorithm. We now monitor the reduction in the relative residual in the l_2-vector norm which is defined as $\|x\|_2=(\Sigma_{j=1}^{n}|x_j|^2)^{1/2}$. We consider one voltage point calculation in case of the EGDM. In Fig. 10 the norm of the relative residual in dependence of the number of iterations for an applied voltage of 5 V is shown in a log-log representation. Newton's algorithm reaches the convergence criterion within a few iterations whereas the convergence of Gummel's algorithm extends over more iterations. The reduction in the residual with Gummel's method is strong initially but then slows down compared to Newton's method.

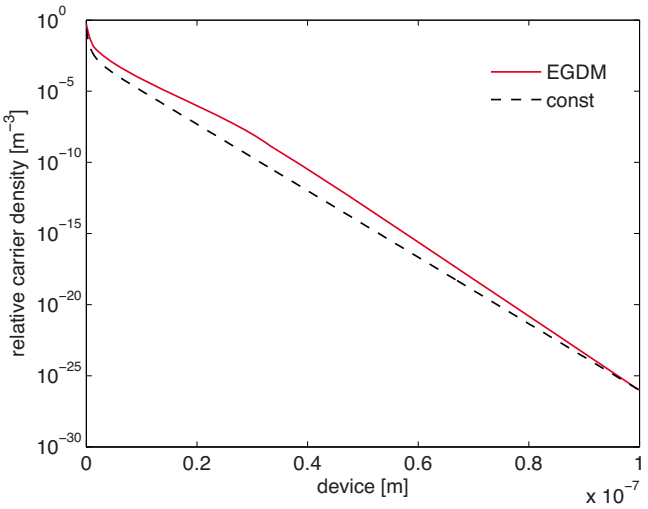

FIG. 8. (Color online) Relative carrier density for a single-layer device of length $l=100$ nm, $n(x=0)=0.5\times10^{27}$ m^{-3} at $T=298$ K with $\hat{\sigma}=6$ and $N_0=10^{27}$ m^{-3}, $\epsilon_r=3$. The dashed lines represent the constant mobility and diffusion solution, the full lines the EGDM result. The built-in voltage is 1.5 V and 2 V, respectively. No external field is applied to the device for the initial guess.

VI. CONCLUSIONS

We have developed efficient methods for the numerical simulation of charge transport in disordered organic semi-

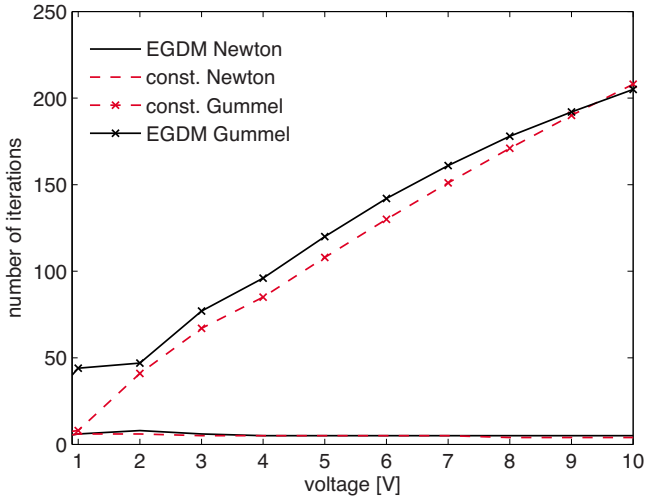

FIG. 9. (Color online) Illustration of number of iterations until convergence is obtained per voltage point. The EGDM and constant mobility case are monitored for Newton and Gummel's algorithm.

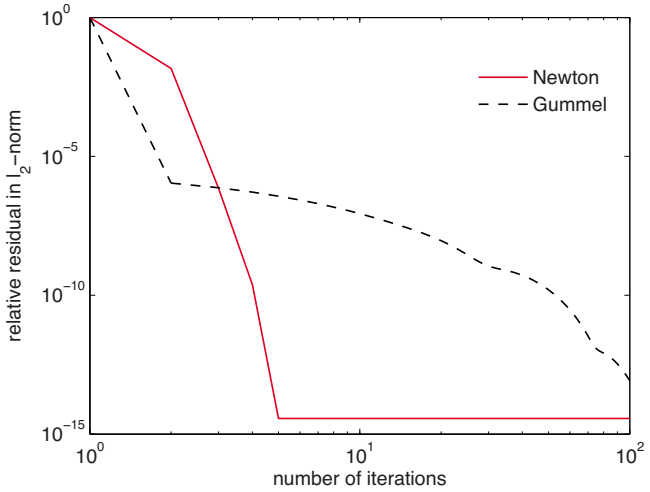

FIG. 10. (Color online) Illustration of the relative residual in l_2-norm for Newton and Gummel's algorithm applied to the EGDM at V_{app}=5 V.

conductor devices. The methods are able to deal with the EGDM including the generalized Einstein relation. We have shown that the numerical drift-diffusion model presented here simulates disordered organic semiconductors in OLEDs correctly. The results of our continuum drift-diffusion model agree favorably with simulation results published by van der Holst[29] who used a 3D master equation model to simulate carrier injection and by van Mensfoort[9] who applied a different continuum approach.

To our knowledge, for the first time, simulation and performance results of a fully-coupled Newton approach for solving the drift-diffusion problem in organic semiconductor have been reported. The new physical models introduce extra nonlinearities and a stronger coupling into the system of equations due to the disorder of the organic semiconductor. Nevertheless, our simulator can deal with a large range of values for the parameters such as voltage, disorder, temperature and trap parameters. This is a significant improvement with respect to time-dependent, decoupled algorithms that tend to be rather time consuming especially at low voltages. The convergence for the EGDM requires only very few iterations for Newton's algorithm. This demonstrates that the system of equations can be solved efficiently despite the advanced transport models used.

Moreover, we have shown in this paper how a good starting point for the equilibrium condition can be calculated. This procedure is also applicable to transient simulations where a device in equilibrium is perturbed by an externally applied field. Further, a good starting point is particularly useful for Newton's algorithm to converge, especially in the disordered case.

We have shown that Newton's method is very valuable for fast current-voltage calculations due to the few iterations per voltage point. In combination with parameter optimization methods this will be used to efficiently characterize organic semiconductor materials on the basis of measured data. The method can also be used for multilayer devices. This, however, requires a correct description of the organic–organic interfaces which is not within the scope of this paper. The numerical framework presented here can also be extended by the exciton rate equation.

ACKNOWLEDGMENTS

We wish to thank R. Coehoorn (Philips Research Eindhoven), W. H. A. Schilders (TU Eindhoven), and R. Hiptmair (ETH Zurich) for fruitful discussions. We acknowledge financial support of the European Community's Seventh Framework program under Grant Agreement No. 213708 (aeviom.eu).

[1] C. Tang and S. VanSlyke, Appl. Phys. Lett. **51**, 913 (1987).
[2] J. H. Burroughes, D. D. C. Bradley, A. R. Brown, R. N. Marks, K. Mackay, R. H. Friend, P. L. Burn, and A. B. Holmes, Nature (London) **347**, 539 (1990).
[3] J. C. Scott and G. G. Malliaras, Chem. Phys. Lett. **299**, 115 (1999).
[4] B. K. Crone, P. S. Davids, I. H. Campbell, and D. L. Smith, J. Appl. Phys. **87**, 1974 (2000).
[5] P. W. M. Blom, M. J. M. de Jong, and J. J. M. Vleggaar, Appl. Phys. Lett. **68**, 3308 (1996).
[6] H. Bässler, Phys. Status Solidi B **175**, 15 (1993).
[7] H. Houili, E. Tutis, H. Lütjens, M. N. Bussac, and L. Zuppiroli, Comput. Phys. Commun. **156**, 108 (2003).
[8] R. Coehoorn and S. L. M. van Mensfoort, Phys. Rev. B **80**, 085302 (2009).
[9] S. L. M. van Mensfoort and R. Coehoorn, Phys. Rev. B **78**, 085207 (2008).
[10] B. Ruhstaller, S. A. Carter, S. Barth, H. Riel, W. Riess, and J. C. Scott, J. Appl. Phys. **89**, 4575 (2001).
[11] B. Ruhstaller, T. Beierlein, H. Riel, S. Karg, J. C. Scott, and W. Riess, IEEE J. Sel. Top. Quantum Electron. **9**, 723 (2003).
[12] J. Staudigel, M. Stößel, F. Steuber, and J. Simmerer, J. Appl. Phys. **86**, 3895 (1999).
[13] Semiconducting thin film optics simulator (SETFOS) with transient and steady-state solver by Fluxim AG, URL: www.fluxim.com
[14] C. Pflumm and U. Lemmer, Quantum Electron. **44**, 790 (2008).
[15] J. C. deMello, J. Comput. Phys. **181**, 564 (2002).
[16] L. J. A. Koster, E. C. P. Smits, V. D. Mihailetchi, and P. W. M. Blom, Phys. Rev. B **72**, 085205 (2005).
[17] J. C. Blakesley, H. S. Clubb, and N. C. Greenham, Phys. Rev. B **81**, 045210 (2010).
[18] J. S. Bonham and D. H. Jarvis, Aust. J. Chem. **30**, 705 (1977).
[19] J. S. Bonham and D. H. Jarvis, Aust. J. Chem. **31**, 2103 (1978).
[20] P. Langevin, Ann. Chim. Phys. VII **28**, 433 (1903).
[21] W. F. Pasveer, J. Cottaar, C. Tanase, R. Coehoorn, P. A. Bobbert, P. W. M. Blom, D. M. de Leeuw, and M. A. J. Michels, Phys. Rev. Lett. **94**, 206601 (2005).
[22] Y. Roichman and N. Tessler, Appl. Phys. Lett. **80**, 1948 (2002).
[23] Y. Preezant and N. Tessler, J. Appl. Phys. **93**, 2059 (2003).
[24] P. Emtage and J. J. O'Dwyer, Phys. Rev. Lett. **16**, 356 (1966).
[25] D. L. Scharfetter and H. K. Gummel, IEEE Trans. Electron Devices **16**, 64 (1969).
[26] J. Rogel-Salazar, D. D. C. Bradley, J. R. Cash, and J. C. deMello, **11**, 1636 (2009).
[27] H. K. Gummel, IEEE Trans. Electron Devices **11**, 455 (1964).
[28] S. Selberherr, *Analysis and Simulation of Semiconductor Devices* (Springer, Vienna, 1984).
[29] J. J. M. van der Holst, M. A. Uijttewaal, R. Ramachandhran, R. Coehoorn, P. A. Bobbert, G. A. D. Wijs, and R. A. D. Groot, Phys. Rev. B **79**, 085203 (2009).
[30] S. L. M. van Mensfoort, J. Billen, S. I. E. Vulto, R. A. J. Janssen, and R. Coehoorn, Phys. Rev. B **78**, 085208 (2008).